Indian Journal of Chemistry
Vol. 62, May 2023, pp. 498-505
DOI: 10.56042/ijc.v62i5.1454

A homogeneous polypyridine-based manganese catalytic system: Reducing CO_2 to CO under visible light

Yu-mei Chen, Ke-Xin Zhou, Quan-Qing Xu* and Zhi-Yang*

Faculty of Chemistry and Chemical Engineering, Yunnan Normal University, Kunming 650 050, PRChina

*E-mail: qqxu1977@163.com (QQX), yangzhi@ynnu.edu.cn (Z-Y)

Received 17 September 2022; Accepted (revised) 21 April 2023

To study the effects of substituent electron - donor on the efficiency of manganese - based photocatalyst, four different Mn(II) complexes have been used as catalysts, the ligands including phenanthroline with methyl and phenanthroline without methyl, bipyridine with methyl and bipyridine without methyl. $[Ru(bpy)_3]^{2+}$ ([Ru]) has been used as a photosensitizer with triethanolamine (TEOA) in CH_3CN solution for the photochemical reduction of CO_2 to CO under visible light irradiation. The turnover numbers of the four catalysts are found to be 99, 717, 167, and 1038, respectively. The experiments have revealed that the catalytic effects of phenanthroline-type complexes are superior to the dipyridyl-type complexes, which has no methyl groups on their ligand. For both phenanthroline-type and dipyridyl-type complexes, the catalysts with a methyl group on the ligand shows good performance than those without a methyl group. The phenanthroline-type complexes with methyl groups has displayed the best catalytic activity among these four catalysts.

Keywords: Photocatalysis, CO_2-CO, Manganese complexes, Homogeneous catalysis

Excessive CO_2 emissions lead to greenhouse effect, and simulating photosynthesis to convert carbon dioxide into high value-added products has become one of the research hotspots[1,2]. CO_2 is used as a feedstock and converted into CO[3,4], CH_4[5], CH_3OH[6], HCOOH[7], and other valuable chemicals; however, the relatively inert C=O bond in the linear O=C=O molecule has a high dissociation energy (>805 $kJ{\cdot}mol^{-1}$)[8]. To achieve high-efficiency and selective CO_2 reduction, noble metals such as Ir[9], Ru, Re[10], and Ir-Re complexes[11] have been used as catalysts with good results; however, designing economically viable, environmentally responsible, and sustainable catalysts using Fe[12], Co[13,14,15], Ni[16], and Mn[17,18] should be a focus of practical applications.

The discovery of ligands is the core challenge of photocatalysis[19]. Recent examples of CO_2 photoreduction catalysts have been exclusively limited to bidentate α-dimmine[20] ligands and bipyridine[21]. There are few reports of the photocatalytic reduction of CO_2 using Mn-based catalysts with electron-donating group substituting phenanthroline ligands.

Herein, we report four photocatalyst complexes, **Mn-bpy** (Fig. 1a), **Mn-dmbpy** (Fig. 1b), **Mn-phen** (Fig. 1c), and **Mn-tmphen** (Fig. 1d), which were synthesized by combining different pyridine ligands with manganese as the central metal. In our photocatalytic systems, [Ru] was used as the photosensitizer and BIH as the sacrificial agent in a mixed solvent CH_3CN/TEOA (V: V = 7: 1) with blue LED lamp irradiation (λ = 420 nm). The experimental results showed that the catalytic effect of complex catalyst with phenanthroline ligands substituted by electron-donating group is better than the Mn-based catalysts previously reported in the literatures, and the CO selectivity reached 99.8%.

Experimental Details

All chemicals were purchased from company such as Sigma-Aldrich and used as received.

Synthesis of Mn-bpy

2,2'-Bipyridine (222 mg, 0.71 mmol) and $[Mn(CO)_5Br]$ (199 mg, 0.72 mmol) were dissolved in 30 mL of diethyl ether, stirred, and then heated under reflux for 3 h. After cooling to room temperature, a yellow powder was obtained, which was filtered, washed with diethyl ether, and then dried under vacuum. Yield: 312 mg (0.59 mmol) (83.4%). ^{1}H NMR (500 MHz, DMSO-d_6, ppm): δ 9.16 (s, 4H), 8.62 (s, 5H), 8.19 (s, 4H), 7.69 (s, 4H). Elemental analysis results for **Mn-bpy**: calculated: C, 45.57; H, 3.06; N, 10.63; found: C 45.19, H 3.04, N 10.49.

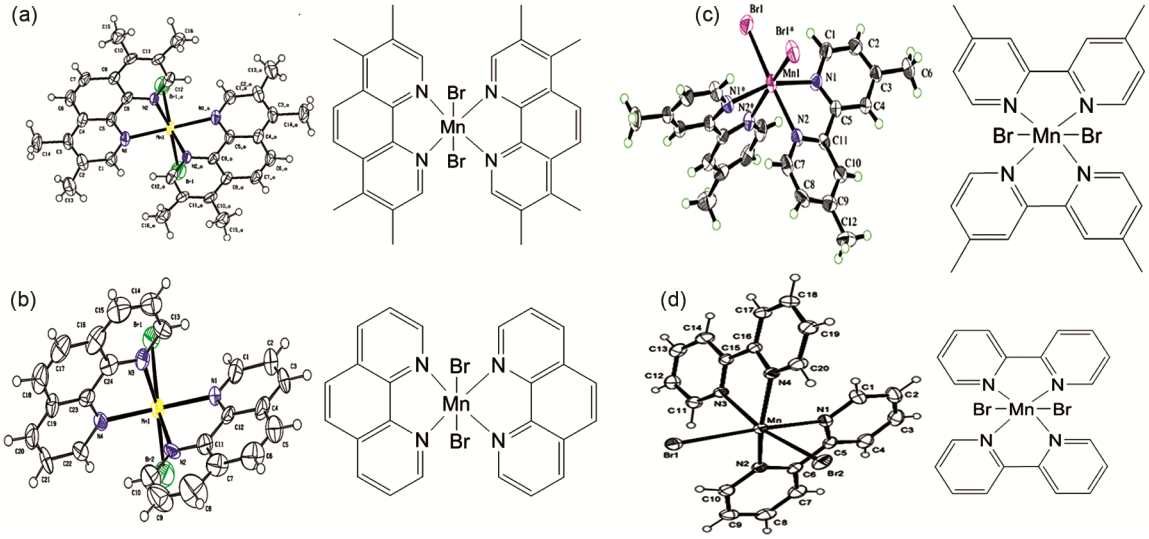

Fig. 1 — Crystal structure diagram of the four catalyst (a) **Mn-bpy**, (b) **Mn-dmbpy**, (c) **Mn-phen**, (d) **Mn-tmphen**

Synthesis of Mn-dmbpy

4,4-Dimethyl-2,2-bipyridine (130 mg, 0.71 mmol) and $[Mn(CO)_5Br]$ (113 mg, 0.41 mmol) were dissolved in 30 mL of diethyl ether, stirred, and maintained under reflux for 2 h. After cooling to room temperature, a yellow powder was obtained by precipitation, which was then washed with ether and dried under vacuum. Yield: 184 mg (0.32 mmol) (90.1%). ^{1}H NMR (500 MHz, DMSO-d_6): δ 8.95 (s, 4H), 8.48 (s, 4H), 7.50 (s, 4H), 2.48 (s, 12H). Elemental analysis results of **Mn-dmbpy**: calculated: C 49.43, H 4.15, N 9.61; found: C 49.06, H 4.06, N 9.49.

Synthesis of Mn-phen

1,10-Phenanthroline (232 mg, 1.29 mmol) and $[Mn(CO)_5Br]$ (200 mg, 0.72 mmol) were dissolved in 50 mL of methanol stirred for 2 h. A yellow powder was obtained by precipitation, which was washed with methanol and then dried under vacuum. Yield: 340 mg (0.59 mmol) (92.4%). ^{1}H NMR (500 MHz, DMSO-d_6, ppm): δ 9.55 (s, 4H), 8.33 (s, 4H), 8.24 (s, 4H), 8.05 (s, 4H). Elemental analysis results for **Mn-phen**: calculated: C 50.12, H 2.80, N 9.74; found: C 49.56, H 2.78, N 9.27.

Synthesis Mn-tmphen

3,4,7,8-Tetramethyl-1,10-phenanthroline (343.8 mg, 1.45 mmol) and $[Mn(CO)_5Br]$ (200 mg, 0.72 mmol) were dissolved in 50 mL of methanol stirred for 2 h. A yellow powder was obtained by precipitation, which was washed with methanol and dried under vacuum. Yield: 460 mg (0.67 mmol) (92.9%). ^{1}H NMR (500 MHz, $CDCl_3$): δ 8.92 (s, 4H), 8.03 (s, 4H), 2.72-2.52 (m, 24H). Elemental analysis results for **Mn-tmphen**: calculated: C 55.92, H 4.69, N 8.15; found: C 55.56, H 4.58, N 8.28.

Characterization results of the catalysts, crystallographic data collection and refinement, experimental details for photocatalytic CO_2 reduction along with results and isotopic labelling experiment procedure along with results are given in Supplementary Information (SI) .

Results and Discussion

The primary crystallographic data for the catalysts are listed in Table S1 (SI). Single-crystal X-ray diffraction (XRD) analysis showed that the four catalysts had different structures. The structures of the complexes **Mn-tmphen** and are novel and have not been previously reported. Although the structure of **Mn-bpy**[22], **Mn-dmbpy**[23] and **Mn-phen**[24] have been reported before, these studies prepared the catalysts in several steps. Herein, we obtained the product **Mn-bpy, Mn-dmbpy, Mn-phen** with similar crystal structure by a direct synthesis method in a different solvent and with higher yields.

The powder X-ray diffraction (PXRD) patterns of four catalysts were recorded at room temperature. Figs S2a-d (SI) show that the PXRD patterns of four complexes synthesized, indicating that single phases of complexes were formed.

To evaluate the reducing capacity of **Mn-bpy**, **Mn-dmbpy**, **Mn-phen**, and **Mn-tmphen** photocatalysts for photocatalytic reduction of CO_2, cyclic voltammetry (CV) curves of deaeration and CO_2 saturation of **Mn-bpy**, **Mn-dmbpy**, **Mn-phen**, and

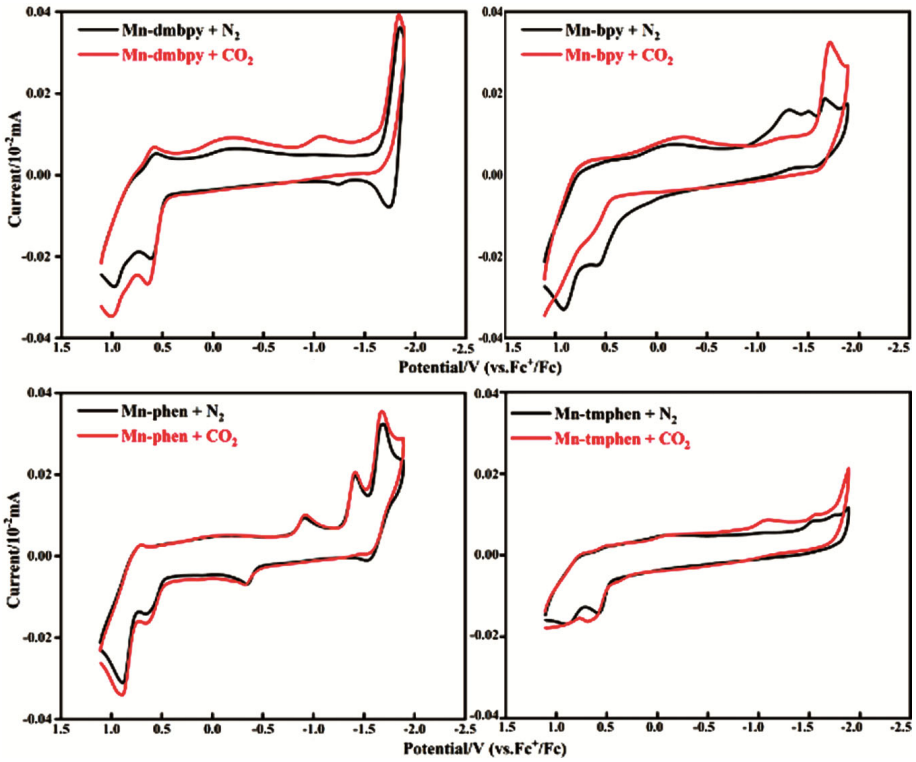

Fig. 2 — Cyclic voltammetry curves of (a) **Mn-bpy**, **(b) Mn-dmbpy,** (c) **Mn-phen** and (d) **Mn-tmphen** in dry acetonitrile. The catalysts concentration was 1 mM, anhydrous $^{n}Bu_4NPF_6$ was used as the supporting electrolyte and acetonitrile was used as the solvent, the scanning speed was 100 mV/s

Mn-tmphen were measured under the same conditions. In a N_2 atmosphere, all these four catalysts showed two irreversible reduction peaks of Mn^{II}/ Mn^{I}(-1.07 ~ -1.56V vs. Fc^{+}/Fc) and Mn^{I}/ Mn^{0} (-1.67 ~ -1.84V vs. Fc^{+}/Fc). Compared with the peak currents under N_2 atmosphere, the intensity of the peak current increased with CO_2 introduction, indicating these four catalysts are potential efficient redox reaction catalysts for CO_2 reduction (Fig. 2). For **Mn-tmphen**, the irreversible reductive peaks were found at Epc = 1.56 V and -1.75 V[25]. For **Mn-bpy, Mn-dmbpy** and **Mn-phen**, these peaks are at -1.32 V and -1.67 V (vs. Fc^{+}/Fc)[26], -1.07 V and -1.84 V (vs. Fc^{+}/Fc)[7], -1.41 V and -1.69 V [27], respectively. Under a N_2 atmosphere, the reduction potential of **Mn-dmbpy** was more negative than **Mn-bpy**. This indicates that the **Mn-dmbpy** complex is easier to donate electrons to CO_2 than **Mn-bpy**. Similarly, the reduction potential of **Mn-tmphen** was more positive than **Mn-phen**. This indicates that the **Mn-tmphen** complex is easier to donate electrons to CO_2 than **Mn-phen**. We have tentatively classified this behaviour to the electron-donating methyl groups on **Mn-dmbpy** and **Mn-tmphen**.

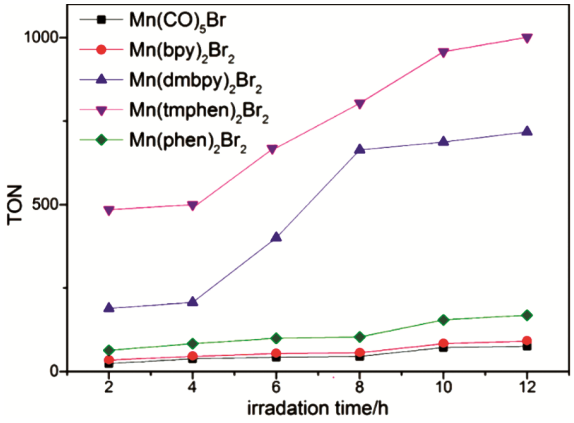

Fig. 3 — Photocatalytic experimental results using the synthesized catalysts. All photocatalytic experiments were performed in a CH_3CN / TEOA (7 : 1 *V* : *V*, 6 mL total) solution with 0.1 mM catalyst, 0.45 mM **[Ru]**, 0.052 M BIH, saturated with CO_2, and irradiated with 460 nm blue light (unless otherwise noted)

After 12 h of illumination of the photocatalytic system (as shown in Figs 3, 4 and Fig. S3.), the results indicate that **Mn-tmphen** had a stronger catalytic effect than **Mn-phen**, **Mn-dmbpy** and **Mn-bpy**. Moreover, no HCOOH was found in the reaction product by high-performance liquid chromatography.

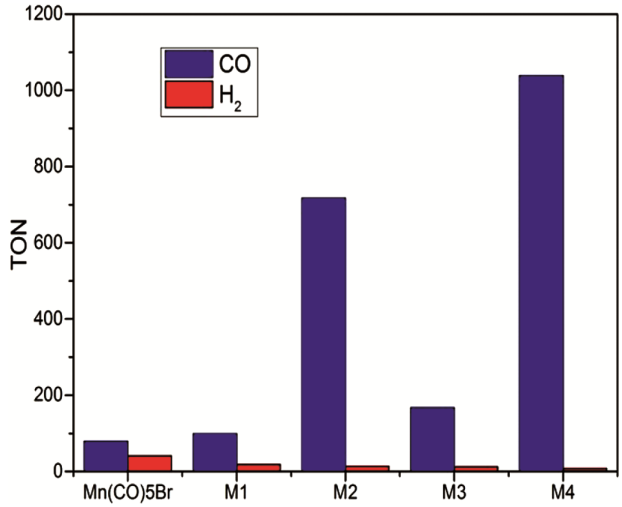

Fig. 4 — Comparison of photocatalytic reduction of CO_2 with different Manganese catalysts. (M1 = **Mn-bpy**, M2 = **Mn-dmbpy**, M3= **Mn-phen**, and M4 = **Mn-tmphen**). Experimental conditions are same as mentioned Fig. 3

Table 1 summarizes the results of the photocatalytic reactions. We used three different mixed solvents, propylene carbonate (PC), acetonitrile (CH_3CN), and N,N-dimethylformamide (DMF), in which PC is a new solvent that strongly adsorbs carbon dioxide. Out of the three solvents, the catalytic efficiency in PC was the best, but its selectivity was poor. In terms of selectivity and efficiency, CH_3CN was the best solvent. The selectivity of the photocatalytic system to CO in CH_3CN-TEOA was higher than that in DMF-TEOA and PC-TEOA (which produced more H_2). This indicates that the photochemical mechanism possibly involved solvent interactions. In the control reactions with the DMF-TEOA solvent system (entries 6-11), we noticed that a small amount of CO was produced in the absence of catalyst because the **[Ru]** photosensitizer has catalytic activity. In the absence of TEOA, CO was not detected (entry 20), which indicates that TEOA is essential for CO production in CH_3CN. In addition, CO was not observed in the CH_3CN-TEOA system in the dark (entry 18). Entries 14 and 15 indicated that the interactions between CH_3CN and TEOA were important for catalytic CO production. However, solvent decomposition alone cannot explain the large difference in the product distribution between the two solvent systems. Overall, the photosensitizer, photocatalyst, and sacrificial reductant were indispensable for the entire photocatalytic system. Solvent interactions were also important, but must be considered with other factors. This was also observed in the CH_3CN-TEOA solvent, in which $Mn(CO)_5Br$ catalytically reduced CO_2. After including a series of pyridine ligands, the catalytic effect gradually increased, and the phenanthroline ligand had a better catalytic effect than the bipyridine ligand, and the catalytic efficiency of the 3,4,7,8-tetramethyl-1, 10-phenanthroline ligand was the best. After 12 h irradiation, the TON_{CO} reached 1038.

Fig. S3 (SI) shows that the yield of CO decreased after 12 h of continuous illumination in the photocatalytic system. When the same amount of **[Ru]** was added again, the system continued to produce CO. Compared with the first stage, the yield of CO decreased. After adding **[Ru]** again, there was a similar trend. This indicates that the catalyst **Mn-tmphen** is stable in the photocatalytic system, and its limiting factor is caused by the decomposition of **[Ru]** rather than the instability of the catalyst.

Fig. 5 shows the UV-visible electronic absorption spectra of **[Ru]** during photocatalysis in TEOA and CH_3CN mixed solvent. In the solution of CH_3CN: TEOA = 7: 1 (*V*/ *V*), the $\lambda_{max}$of **[Ru]** was 455 nm. The broad low-energy band near 455 nm corresponded to the metal-to-ligand charge transition ($d\pi \rightarrow \pi^*$)[21]. Upon increasing the photolysis time, **[Ru]** decomposed rapidly in the absence of **Mn-tmphen**. However, when **Mn-tmphen** was added to the system, the decomposition of **[Ru]** was sluggish, which is consistent with previous literature reports[28,7]. Fig. S4 (SI) showed the similar degradation behaviour of **[Ru]** with **Mn-dmbpy** as the catalyst.

The calculated energy levels of **Mn-tmphen** and **Mn-phen** for bonding to CO_2 are shown in Fig. 6. The energy gap from the HOMO of the catalyst to the LUMO of CO_2 for **Mn-tmphen** was 3.68 eV and **Mn-phen** was 4.20 eV. The result of 3.68 eV < 4.20 eV indicate that **Mn-tmphen** transferred electrons to CO_2 is more easily than**Mn-phen**. **Mn-tmphen**, with methyl groups, more easily combined with CO_2. The calculated HOMO-LUMO band gap of the monomer **Mn-tmphen** is 2.57eV, and **Mn-phen**is 2.40 eV, nearly in accord with the measured absorption energy results 2.58 eV and 2.43 eV, hereon, we think that the low-energy absorption comes from the mixed-orbital parentage involving intra-ligand charge transfer (ILCT) and metal-to-ligand charge transfer (MLCT). These results revealed that the electron-donating methyl groups give them an advantage in providing electrons for CO_2 catalysis. Similarly, the corresponding conclusions can be drawn from Fig. S5 (SI).

Table 1 — Control experimental results from Fe_2-DMBPY and Fe_2-BPY for photocatalytic conversion of CO_2 to CO

Entry	[cat]	[Ru]/mM	[BIH]/mM	TON_{CO}	TON_{H2}	$Selectivity_{CO}$
Catalytic Experiments in DMF-TEOA, DMF-TEOA and CH_3CN-TEOA, respectively						
1[abc]	$Mn(CO)_5Br$	0.45	0.052	0.0	0	0
2[abc]	**Mn-bpy**	0.45	0.052	0.0	0	0
3[abc]	**Mn-dmbpy**	0.45	0.052	0.0	0	0
4[abc]	**Mn-phen**	0.45	0.052	0.0	0	0
5[abc]	**Mn-tmphen**	0.45	0.052	0.0	0	0
Catalytic Experiments in DMF-TEOA						
6	$Mn(CO)_5Br$	0.45	0.052	21.0	8	72.4%
7	**Mn-bpy**	0.45	0.052	35.0	7	83.3%
8	**Mn-dmbpy**	0.45	0.052	110.0	2.8	97.5%
9	**Mn-phen**	0.45	0.052	40.0	3	93.0%
10	**Mn-tmphen**	0.45	0.052	351.0	1.9	99.5%
11[e]	0	0.45	0.052	7.2	0.6	92.3%
Catalytic Experiments in CH_3CN-TEOA						
12	$Mn(CO)_5Br$	0.45	0.052	79.0	41.0	65.8%
13	**Mn-bpy**	0.45	0.052	99.0	18.8	84.0%
14	**Mn-dmbpy**	0.45	0.052	717.0	13.3	98.2%
15	**Mn-phen**	0.45	0.052	167.0	12.2	93.2%
16	**Mn-tmphen**	0.45	0.052	1038.0	8.1	99.2%
17[a]	**Mn-dmbpy**	0.45	0.052	0.0	0.0	0
13[b]	**Mn-dmbpy**	0.45	0.052	0.0	0.0	0
14[c]	**Mn-dmbpy**	0	0.052	0.0	0.0	0
18[d]	**Mn-dmbpy**	0.45	0.052	0.0	0.0	0
19[e]	0	0.45	0.052	7.5	0.4	94.9%
Catalytic Experiments in PC-TEOA						
20	$Mn(CO)_5Br$	0.45	0.052	40.2	49.0	45.1%
21	**Mn-bpy**	0.45	0.052	58.2	36.3	61.6%
22	**Mn-dmbpy**	0.45	0.052	254.6	28.0	90.1%
23	**Mn-phen**	0.45	0.052	40.0	29.0	58.0%
24	**Mn-tmphen**	0.45	0.052	469.0	8.0	98.3%
25[e]	0	0.45	0.052	30.0	8.6	77.7%

All runs were irradiated with 470 nm blue light. The catalytic system had a catalyst concentration of 0.1 mM, an irradiation time of 12 h, [a]without CO_2, [b]in the dark, [c]without **[Ru]**, [d]without TEOA, and [e]without catalyst. TON_{CO} = n (mol CO) / n (mol catalyst); $Selectivity_{CO}$ = n (mol CO) / n (mol CO + mol H_2).

High-resolution mass spectrometry (HRMS) was applied to monitor the intermediates generated during photocatalysis using the **Mn-tmphen** catalyst. Fig. 7 shows the signals of the three fragments of **Mn-tmphen** (m/z = 366.2600, 367.2900) in positive-ion mode. The peaks at m/z = 749.5023 and 571.2523 corresponded to $\mathbf{[Ru]^{2+}}$and $\mathbf{[Ru]^{+}}$(Fig. S6a to Fig. S6b), respectively. The peaks at m/z = 767.5004, m/z = 338.1833, m/z = 378.1251, m/z =307.2044 and m/z = 360.1143 were attributed to the intermediates $\mathbf{[Mn + K^{+} + TEOA]^{+}}$, $\mathbf{[Mn + TEOA]^{2+}}$,$\mathbf{[Mn + H^{+} + TEOA]^{+}}$, $\mathbf{[Mn + 2CO + TEOA]^{2+}}$ and $\mathbf{[Mn + 2HCO + TEOA]^{2+}}$ (Fig. S6c to Fig. S6f), respectively.

The $^{13}CO_2$ isotopic labeling experiments were adopted using GC-MS. The photocatalytic gas product was injected and then separated. Fig. S8 shows the GC-MS chromatograms of the peaks at m/z = 29.0 (^{13}CO). Herein, the peak at m/z = 45.2 attributed to $^{13}CO_2$, and the peak at m/z = 28.0 attributed to N_2 or small amount of ^{12}CO. The product CO was verified by isotopic labeling experiment that it is derived from CO_2 when using $^{13}CO_2$ as the substrate gas.

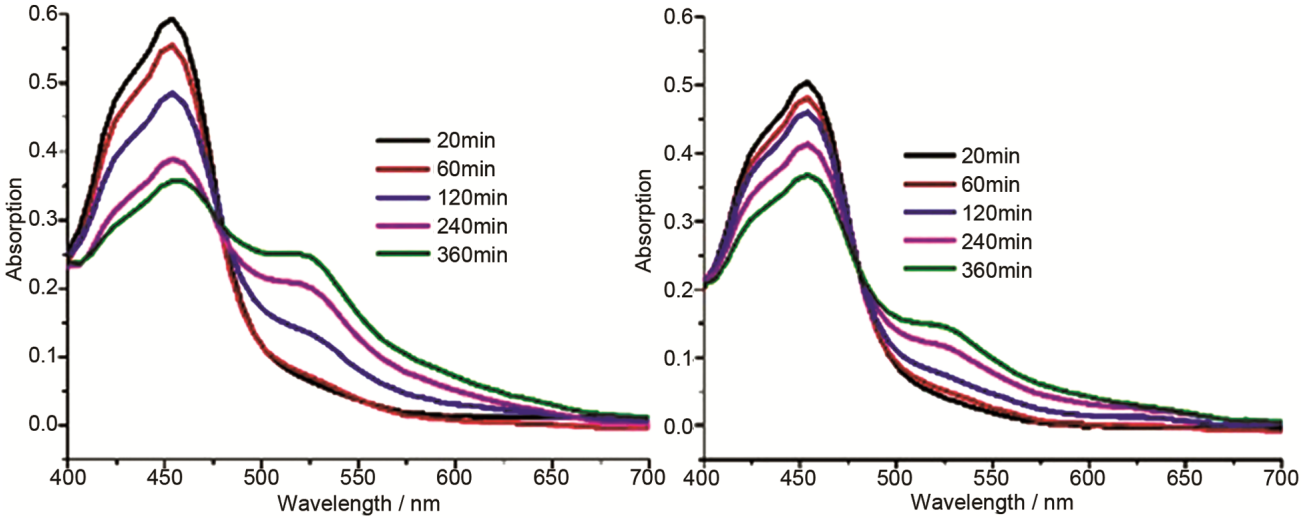

Fig. 5 — The electronic absorption spectra at different irradiation times: **[Ru]** (4×10^{-5} M); solvent was CH_3CN: TEOA = 7: 1 (*V* / *V*), [A]without catalyst **Mn-tmphen** and [B]with catalyst **Mn-tmphen** (1×10^{-5} M); the blue lamp produced a spectrum within the range of 460 ≤ λ ≤ 465 nm.Each sample were deaerated with N_2 before measuring the emission spectra

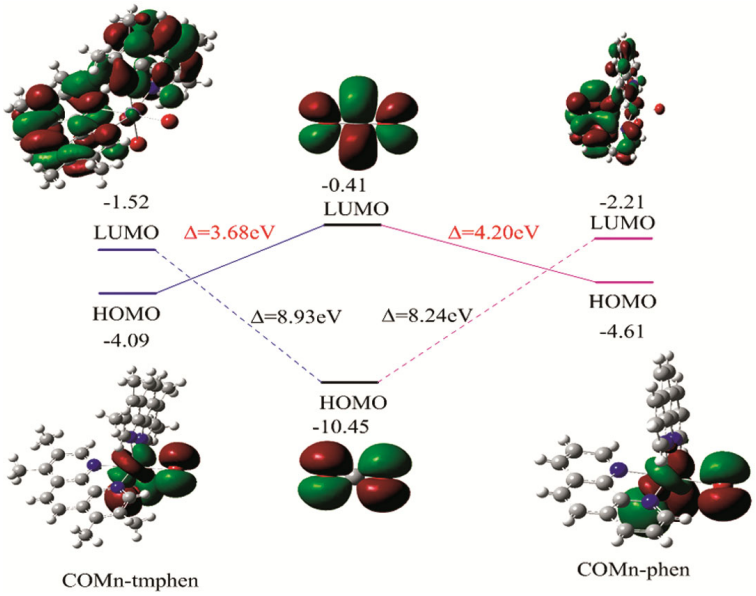

Fig. 6 — Contour plots and orbital energies of the HOMO and LUMO of **Mn-tmphen**, CO_2, and Mn-phen

The number of incident photons, measured using a classical iron ferrioxalate ($K_3Fe(C_2O_4)_3$) chemical actinometer, was 2.01×10^{24} photons per hour. According to quantum yield calculations[29] and using known parameters[30], the quantum yield of CO formation is Φ_{co}= 0.01546 %.

A plausible mechanism for the photocatalytic reduction of CO_2 to CO by the Mn^{II} complexes is shown in Scheme 1. First, $[Ru(bpy)_3]^{2+}$ was excited to $[Ru(bpy)_3]^{2+*}$ via irradiation, and then reduced to the active species $[Ru(bpy)_3]^{+}$ by BIH. After that, the catalyst was reduced by the electrons of $[Ru(bpy)_3]^{+}$, which returned to the initial state of $[Ru(bpy)_3]^{2+}$. For the catalytic reduction of CO_2, the metal catalytic centre manganese underwent the following processes: (1) TEOA bound to the complex through adsorption and the fracture of two Br^- ions; (2) two CO_2 bound to the metal centre by adsorption; (3) CO-Mn-CO was formed from the HCO-Mn-HCO adduct; (4) CO was generated via dissociation, and the catalyst was regenerated. Among them, TEOA can combine with the catalyst through adsorption, and it plays a role as CO_2 absorber[32]. In addition, the main intermediates in the whole catalytic system were **$[CO_2 – Mn – CO_2]^{2+}$,**

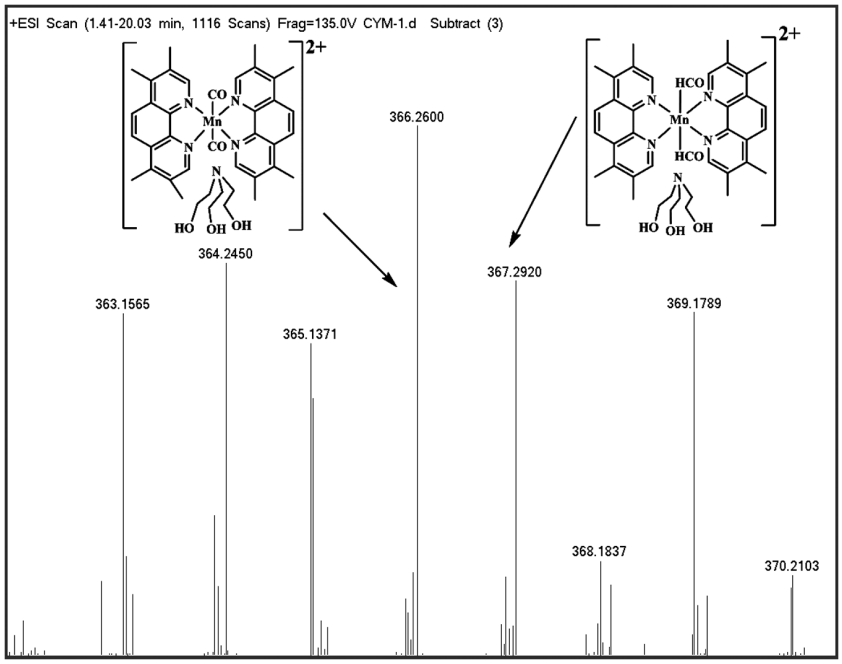

Fig. 7 — HRMS spectra of CO_2-saturated CH_3CN / TEOA solution (V / V = 7 / 1; total = 6 mL) containing 0.100 mM catalyst **Mn-tmphen**, 0.45 mM [Ru], and 0.052 M BIH after irradiation for 2 h

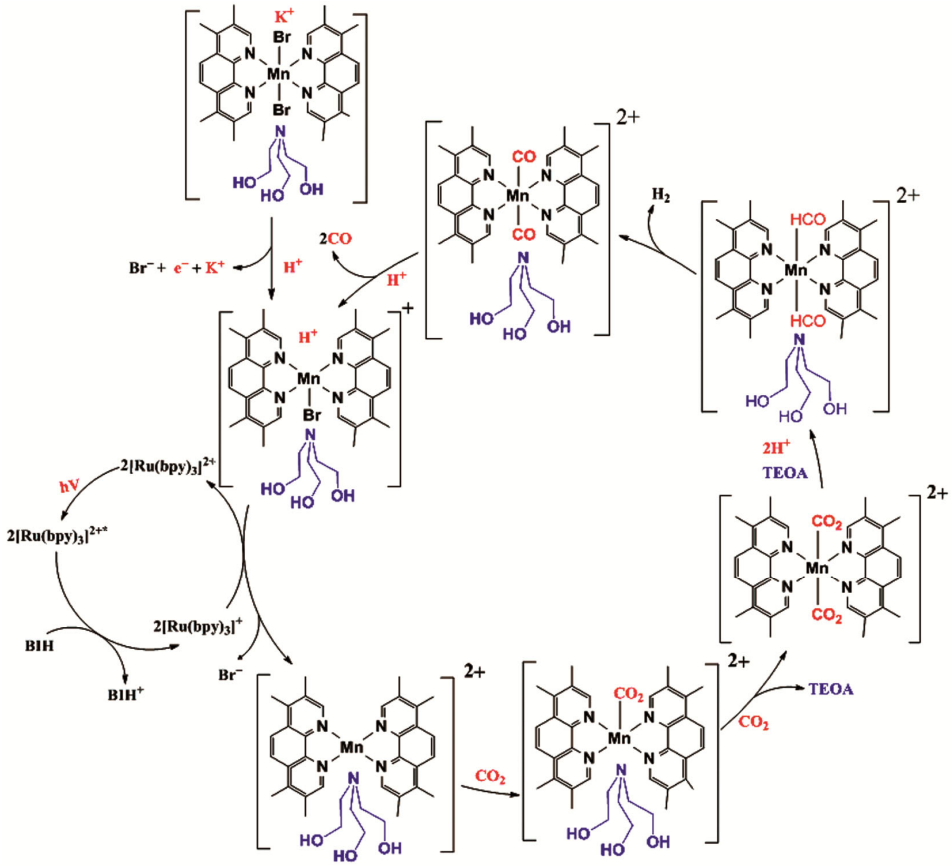

Scheme 1 — Proposed mechanism for the photocatalytic reduction of CO_2 to CO using the **Mn-tmphen**/ **[Ru]** / BIH / TEOA system

$[CO_2 – Mn- TEOA]^{2+}$, $[HCO – Mn– HCO]^{2+}$ and **$[CO – Mn – CO]^{2+}$**, respectively.

Here, four highly efficient, visible-light-driven, and manganese complex catalytic systems were developed to reduce CO_2 to CO. These four complexes were simple, inexpensive, and easy to prepare. The catalytic activity of **Mn-tmphen** was greater than that of the other three catalysts. To our knowledge, the TONs of these **Mn-tmphen** catalysts are the highest reported for manganese-based homogeneous catalysts for the photocatalytic reduction of CO_2 to CO. Notably, these complexes also exhibited high selectivity. Overall, our results provide guidance towards the research and development of other Mn-based catalysts for photocatalytic CO_2 reduction.

Conclusion

Here, four highly efficient, visible-light-driven, and manganese complex catalytic systems were developed to reduce CO_2 to CO. These four complexes were simple, inexpensive, and easy to prepare. The catalytic activity of **Mn-tmphen** was greater than that of the other three catalysts. To our knowledge, the TONs of these **Mn-tmphen** catalysts are the highest reported for manganese-based homogeneous catalysts for the photocatalytic reduction of CO_2 to CO. Notably, these complexes also exhibited high selectivity. Overall, our results provide guidance towards the research and development of other Mn-based catalysts for photocatalytic CO_2 reduction.

Acknowledgement

This work was supported by the National Natural Science Foundation of China (22265032).

Supplementary Information

Supplementary information is available in the website http://nopr.niscpr.res.in/handle/123456789/58776.

References

1 Fu Z, Yang Q, Liu Z, Chen F, Yao F, Xie T, Zhong Y, Wang D, Li J, Li X & Zeng G, *J CO_2 Util*, 34 (2019) 63.
2 Fu J, Jiang K, Qiu X, Yu J & Liu M, *Materials Today,* 32 (2020) 222.
3 Saito D, Yamazaki Y, Tamaki Y & Ishitani O, *J Am Chem Soc*, 142 (2020) 19249.
4 He X, Cao Y, Lang X D, Wang N & He L N, *Chem Sus Chem*, 11 (2018) 3382.
5 Rao H, Lim C H, Bonin J, Miyake G M & Robert M, *J Am Chem Soc*, 140 (2018) 17830.
6 Wu Y A, McNulty I, Liu C, Lau K C, Liu Q, Paulikas A P, Sun C J, Cai Z H, Guest J R, Ren Y, Stamenkovic V, Curtiss L A, Liu Y & Rajh T, *Nat Energy*, 4 (2019) 957.
7 Cheung P L, Machan C W, Malkhasian A Y S, Agarwal J & Kubiak C P, *Inorg Chem*, 55 (2016) 3192.
8 Nguyen H L, *Adv Energy Mat*, 10 (2020) 2002091.
9 Sato S, Morikawa T, Kajino T & Ishitani O, *Angew Chem Int Ed Engl*, 125 (2013) 1022.
10 Hawecker J, Lehn J M & Ziessel R, *J Chem Soc Chem Comm*, (1983) 536. (https://doi.org/10.1039/C39830000536)
11 Kuramochi Y & Ishitani O, *Inorg Chem*, 55 (2016) 5702.
12 Takeda H, Ohashi K, Sekine A & Ishitani O, *J Am Chem Soc*, 138 (2016) 4354.
13 Guo Z G, Cheng S W, Cometto C, Anxolabéhère -Mallart E, Ng S M, Ko C C, Liu G J, Chen L J, Robert M & Lau T C, *J Am Chem Soc*, 138 (2016) 9413.
14 Ma B, Chen G, Fave C, Chen LJ, Kuriki R, Maeda K, Ishitani O, Lau TC, Bonin J & Robert M, *J Am Chem Soc,* 142 (2020) 6188.
15 Zhang L Y, Li S W, Liu H P, Cheng Y S, Wei X W, Chai X & Yuan G, *Inorg Chem*, 59 (2020) 17464.
16 Thoi V S, Kornienko N, Margarit C G, Yang P D & Chang C J, *J Am Chem Soc*, 135 (2013) 14413.
17 Ma X, Zheng L & Bian Z Y, *Chem Eng Sci*, 229 (2021) 116042.
18 Xin X, Ma N, Hu CY, Liang Q & Bian ZY, *Nano*, 14 (2019) 1950024.
19 Hameed Y, Gabidullin B & Richeson D, *Inorg Chem*, 57 (2018) 13092.
20 Rohacova J & Ishitani O, *Chem Sci*, 7 (2016) 6728.
21 Juris A, Balzani V, Barigelletti F, Campagna S, Belser P & Zelewsky A V, Coord Chem Rev, 84 (1988) 85.
22 Hwang I C & Ha K, *Z Kristallogr NCS*, 222 (2007) 209.
23 Sakamoto J, Yoshikawa N, Takashima H, Tsukahara K, Kanehisa N, Kai Y & Matsumura K, Acta Cryst E60 (2004) m352. (https://doi.org/10.1107 /S1600536804004234)
24 Shen X P & Yuan A H, Acta Cryst, E60 (2004) m1074. (https://doi.org/10.1107/S1600536804015983)
25 Roy S S, Talukdar K & Jurss J W, *Chem Sus Chem*, 14 (2021) 662.
26 Sampson M D, Nguyen A D, Grice K A, Moore C E, Rheingold A L & Kubiak C P, *J Am Chem Soc*, 136 (2014) 5460.
27 Islam G J, Akhtar H M N, Mamun M A & Ehsan M Q, J Saudi Chem Soc, 13 (2009) 177.
28 Kuo H Y, Lee T S, Chu A T, Tignor S E, Scholes G D & Bocarsly A B, *Dalton Trans*, 48 (2019) 1226.
29 Montalti A C, Prodi M L & Gandolfi M T, *Handbook of Chemistry*, (CRC Press) 2006. (https://doi.org/10.1201/ 9781420015195).
30 Nie X C, Hu R, Liu R, Zhu A X, Liu F Y, Xu Q Q & Yang Z, *Catal Comm*, 134 (2020) 105861.
31 Park S W, Choi B S & Lee J W, *Korean J Chem Eng*, 23 (2006) 138.